Dynamic properties of spin-orbital correlation effects in the spinel MnV$_2$O$_4$

Hao-Yu Niu ◉, Zhuo Zeng, Yu-Jie Song, Hao Huang, You-Yuan Liang, De-Quan Jiang,
Zhao-Ming Tian, Zhong-Wen Ouyang, and Zheng-Cai Xia ◉*
Wuhan National High Magnetic Field Center and School of Physics of
Huazhong University of Science and Technology, Wuhan 430074, China

The spin-orbital-lattice coupling in spinel MnV$_2$O$_4$ single crystal has been investigated by static field magnetization (field sweep rate of 50 Oe/s), pulsed field magnetization (field sweep rate $\sim 10^5$ kOe/s), dielectric permittivity, and magnetostriction. Experimental results show that the magnetization and magnetostriction are related to the field sweep rate. The analysis of the magnetization, dielectric permittivity and magnetostriction in static magnetic field shows that the collinear (CL) and non-CL (NCL) spin configurations coexist between $T_N \sim 56$ K and $T^* \sim 52$ K, and the NCL spin configuration can be induced by applied magnetic field. In particular, the magnetization and magnetostriction steps associated with CL and NCL transitions observed in the static magnetic field becomes smooth in the pulsed magnetic field, indicating the slow relaxation characteristic of these phase transitions. Based on the orbital state of MnV$_2$O$_4$ and the Kugel-Khomskii model, we propose an quasiadiabatic spin-orbital correlation mechanism in which the interaction between the spin and the t_{2g} orbital of V^{3+} ions is rather weak; this weak interaction results in the magnetic properties of MnV$_2$O$_4$ is related to the field sweep rate.

I. INTRODUCTION

In transition metal compounds, the orbital degrees of freedom of d electron play an important role in electric and magnetic properties. When the number of d electrons is less than the degeneracy of the d orbital, the d electrons are free to choose which d orbital to occupy [1]. When the orbital degeneracy is lifted by the interaction with the lattice, the intriguing phenomenon of orbital ordering (OO) occurs, and the OO can also emerge in the systems with the presence of Kugel-Khomskii interaction. The best-known prototype of OO is the Jahn-Teller (JT) distortion observed in LaMnO$_3$, where the e_g degenerate manifold in the cubic crystal field is lifted by the JT distortion [2]. The underlying physics in OO has been well accounted for by the Kugel-Khomskii model; according to this model, whether the occupied orbitals at neighboring sites are same or not is strongly influenced by whether the neighboring spins are aligned to the same or opposite direction [3,4]. At present, some intriguing phenomena caused by the interaction of spin, orbital, and lattice degrees of freedom have attracted considerable attention in the field of condensed matter physics [5–7].

Spinel vanadium oxides with general formula AV$_2$O$_4$, where A can be either a magnetic or a nonmagnetic species such as Mg, Zn, Cd, Fe, Co, or Mn [8–19], and where the interplay of spin, orbital degrees of freedom of the A and V ions is important, have attracted extensive interest due to a lot of intriguing physical phenomena, such as metal-insulator transition, OO, geometrical frustration, and multiferroicity [20,21].

A typical family member of AV$_2$O$_4$ is MnV$_2$O$_4$, where Mn^{2+} is in a $3d^5$ high spin configuration $S = 5/2$ with quenched orbital angular momentum, and V^{3+} sublattice forms a pyrochlore lattice. The two d electrons of the V^{3+} ion occupy the triply degenerate t_{2g} orbitals with total spin of $S = 1$, leading to the t_{2g} active OO. For OO, most of the attention is focused on systems with partially filled e_g orbitals [2,22,23]. In contrast with the e_g active OO, in which the JT effect is much stronger due to the related d orbitals directly point to ligands [24], t_{2g} active OO shows relatively weaker JT effect, which can compete with the spin-orbital coupling [25]. In addition, the OO in MnV$_2$O$_4$ is more complicated due to the geometrical frustration of pyrochlore lattice. Previous studies have shown that, with the decrease of temperature, MnV$_2$O$_4$ undergoes a paramagnetic (PM) to collinear (CL) ferrimagnetic transition at $T_N \approx 56$ K with the Mn and V spin moments antiparallel. At $T^* \approx 52$ K, a CL to non-CL (NCL) ferrimagnetic transition occurs, accompanied by a cubic-to-tetragonal structural transition induced by the so-called A-type antiferro-OO. Recently, it has been widely accepted that the PM to NCL ferrimagnetic transition and the cubic-to-tetragonal structural transition both occur at $T_N \approx 56$ K, while the origin of the second transition at $T^* \approx 52$ K is still under debate [1,26–33].

Pulsed magnetic field is an ideal tool to study the dynamic properties of magnetic systems because of its ultrafast field sweep rate. In this study, we have systematically investigated the dynamic properties of magnetization, magnetostriction of spinel MnV$_2$O$_4$ single crystal using a pulsed magnet (with the field sweep rate $\sim 10^5$ kOe/s). The magnetization results measured in pulsed magnetic field are different from that measured in static magnetic field, abnormal magnetization and magnetostriction behaviors were observed under the pulsed
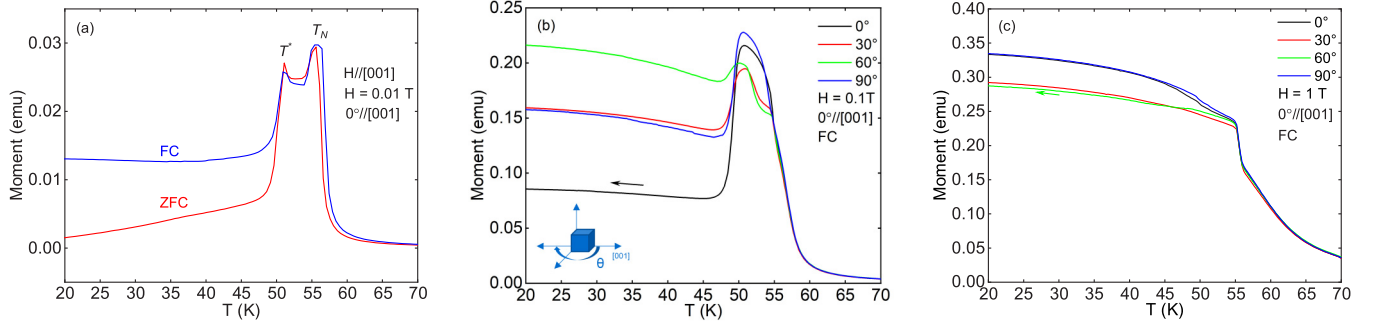
*xia9020@hust.edu.cn

FIG. 1. (a) The magnetic susceptibility of MnV$_2$O$_4$ under $H = 0.01$ T in ZFC and FC. (b), (c) The temperature dependence of magnetic susceptibilities of MnV$_2$O$_4$ under $H = 0.1$ T and $H = 1$ T with different magnetic directions, respectively.

magnetic field, we suggest that an quasiadiabatic process was established due to the rather weak spin-orbital correlation effect in MnV$_2$O$_4$ and the fast field sweep rate of the pulsed magnetic field. Our results also suggest that the NCL and CL phases coexist between T_N and T^*, and that the transition at T^* is closely related to the orbital state of MnV$_2$O$_4$. The experimental results show that this compound provides an ideal playground for the study of the weak spin-orbital interaction in the t_{2g} orbitals, and the pulsed high magnetic field is a powerful tool for the study of the dynamic magnetic properties.

II. EXPERIMENT

Single-crystal samples of MnV$_2$O$_4$ were grown using the optical float-zone method [27]. X-ray powder diffraction was used to determine the crystalline quality and Laue x-ray diffractometer was used to determine the crystalline orientation. From the fact that the three principal crystalline axes are equivalent in the cubic structure, we simply define one of the major axes as $[001]_c$ for subsequent measurements. For magnetic measurements, superconducting quantum interference device (SQUID) and a pulsed magnet were used. The dielectric permittivity measurements were performed by 6500B precision impedance analyzers combined with a physical property measurement system. Silver paint electrodes were placed on opposing parallel sample surfaces which are normal to $[001]_c$, and the AC electric field with frequency of 10 kHz was applied. Resistance-type strain gauges were used to study the magnetostriction effect, the surface of (100) or (010) was attached to the strain gauge, and $[001]_c$ is parallel to the sensing direction of the strain gauge. To eliminate the effects of magnetic and thermal history, the samples were demagnetized at 100 K and cooled from 100 K before each test.

III. RESULTS AND DISCUSSION

The magnetic susceptibility of MnV$_2$O$_4$ is displayed in Fig. 1(a), in which two peaks were observed at T_N and T^*, respectively. It is obvious that a divergence emerges just below T^*, which arises from the glasslike behavior as reported in previous study [34]. Angular dependence of magnetic susceptibility from $[001]_c$ to $[010]_c$ (or $[100]_c$) direction is displayed in Figs. 1(b) and 1(c). In Fig. 1(b), apparently magnetic

anisotropy was observed, as field direction rotates, magnetic susceptibility varies successively but shows no uniformity. This nonuniformity exhibits the complicated spin ordered states at low temperature due to the geometrical frustration of the pyrochlore lattice. To further examine this anisotropic behavior, magnetization measurements were carried out in a magnetic field of 1 T as depicted in Fig. 1(c), in which the difference of susceptibility at different angles is smaller than that in Fig. 1(b), indicating that the anisotropic energy in MnV$_2$O$_4$ is weak and can be partially compressed by higher applied magnetic field. Since the susceptibility above T_N is almost equivalent for all field directions, the observed anisotropy below T_N is intrinsic and may result from spin-orbital coupling in MnV$_2$O$_4$.

The magnetic-field dependence of magnetization measured by the static-state magnetic field at different temperatures is shown in Fig. 2(a). At 4.2 K, the field-induced ferromagnetic transition occurs at the low magnetic-field region, and the saturated moment is about 3.8 μ_B/f.u., which is close to the theoretical value (given later) of the well-known NCL ferrimagnetic magnetic configuration in MnV$_2$O$_4$. Thus we assume that this transition arises mainly from the rotation of the magnetic domain, where the ferrimagnetic configuration between Mn and V sublattices is unchanged. Above T^*, the field-induced saturated moment gradually decreases with increasing temperature. Especially apart from the rotation of the ferromagnetic domain at the low-field regime, an obvious steplike transition with hysteresis loop was observed and the transition field moves toward the higher field regime with increasing temperature. To understand the origin of the steplike transition, we made a simple mathematical calculation using the saturated moments of $m_{\text{Mn}} \approx 4.2$ μ_B and $m_V \approx 1.3$ μ_B and the canted angle about $65°$ of the V moments with respect to the Mn moments in the NCL region [26]. For the CL spin configuration, the net moments $m_{\text{net1}} = m_{\text{Mn}} - 2m_V \approx 1.6$ μ_B/f.u., and for the NCL spin configuration, the net moments $m_{\text{net2}} = m_{\text{Mn}} - 2m_V \cos 65° \approx 3.1$ μ_B/f.u. We found the moments when the magnetic field reached 7 T (~ 3 μ_B) are very close to m_{net2}, and the change of the magnetic moments before and after the steplike transition (~ 1 μ_B) is comparable to the value of $m_{\text{net2}} - m_{\text{net1}} \approx 1.5$ μ_B at T_N. Therefore it is reasonable to assume that the steplike transition is mainly dominated by the field-induced CL to NCL magnetic configuration transition. The greater saturated moments (3.8 μ_B/f.u.) at 4.2 K may be due to the suppression of the thermal
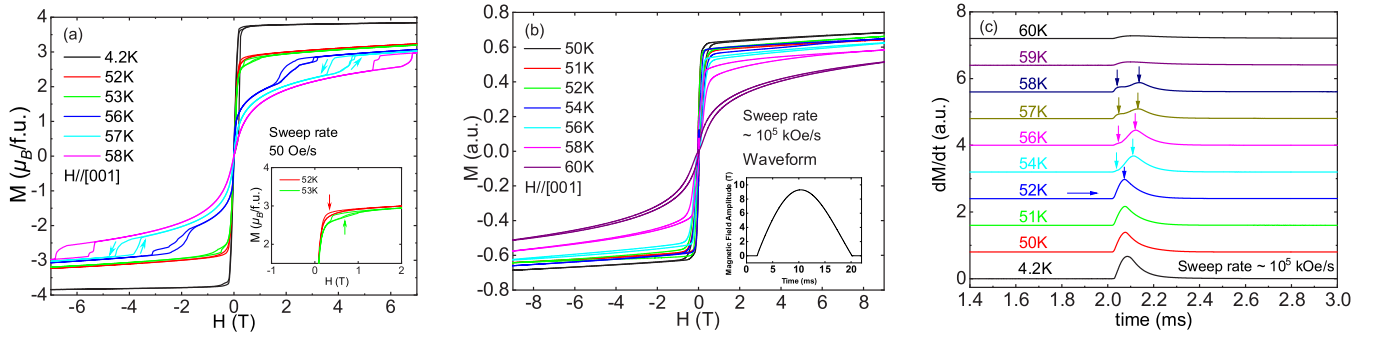
FIG. 2. (a), (b) The magnetic-field dependence of magnetization of MnV_2O_4 measured by static magnetic field and pulsed magnetic field, respectively; the inset in (a) shows the local zoom of the hysteresis loop around T^* and (b) gives the wave form of the pulsed magnetic field used. (c) The derivative signal of magnetization measured by pulsed magnetic field.

fluctuations at low temperature, which makes the spin further ordered. Here the frustrated feature of the pyrochlore structure of the V sublattice makes the CL spin configuration unstable. Therefore the applied magnetic field can partially release the frustration and make it the NCL spin structure which is more stable. A different but comparable situation was encountered in $CdCr_2O_4$ [35] in which a 1/2 magnetization plateau was observed; the plateau state can be ascribed to a CL spin configuration with three-up spins and one-down spin out of four spins of each Cr tetrahedron, and the application of a magnetic field aligns the spins and therefore suppresses the magnetic frustration. In MnV_2O_4, below T_N, the hysteresis loop becomes small and nearly vanishes around T^*, as shown in the inset of Fig. 2(a). This result may indicate that the NCL ferrimagnetic state is not completely reached at T_N. Instead, the CL and NCL magnetic states coexist until T^*, below which the magnetic configuration is totally NCL.

In the case of high sweep field rate, the magnetization curves measured in the pulsed magnetic field are different from that in the static magnetic field. As given in Fig. 2(b), below T^*, the magnetization behavior is similar to that in the static magnetic field. However, above T^*, no significant step-like transition was observed and only a small hysteresis loop appears. Different from the magnetization behavior measured in the static field, the steplike transition in the static magnetic field becomes smooth in the pulsed magnetic field. In order to analyze the dynamic characteristic of the magnetization, the derivative signals of magnetization measured with pulse magnetic field were recorded as shown in Fig. 2(c) in which the field-induced phase transitions are obviously temperature dependent. As the temperature increases, the single peak splits into two peaks, then merges into a single peak and becomes invisible above 59 K. In the magnetization process, the lower field transition may arise from the unpolarized spin components in the PM phase, and the higher field transition may be attributed to the field-induced CL to NCL transition.

In this study, the field sweep rate of the static magnetic field is slow (50 Oe/s), while the field sweep rate of the pulsed magnetic field is much faster ($\sim 10^5$ kOe/s). Detailed field sweep rate measurements are shown in Fig. S1 of the Supplemental Material [36]. Usually high-field sweep rates may delay magnetic phase transition, causing the critical field moves to higher magnetic-field regime; this is the so-called magnetic viscosity [37,38]. However, the situation in

MnV_2O_4 is counterintuitive. Comparing Figs. 2(a) and 2(b), the transition becomes smooth and moves to a much lower field region under pulsed magnetic field, which indicates that the conventional magnetic viscosity is insufficient to explain this anomaly. Therefore a new physical mechanism needs to be introduced. As mentioned earlier, the correlation effect among spin, orbital, charge, and lattice degrees of freedom is complicated in MnV_2O_4. To understand the possible physics behind this abnormal magnetization behavior, we made systematical measurements on dielectric permittivity and strain to explore the role of charge, orbital, and lattice degrees of freedom on the abnormal magnetization behavior.

In order to detect a potential magnetoelectric effect in MnV_2O_4, dielectric permittivity measurements were performed. The temperature dependence of the dielectric permittivity under different magnetic fields is shown in Fig. 3(a). As shown in the inset of Fig. 3(a), with the increase of temperature, a sharp rise of ε' at $T_N \approx 56$ K was observed at zero magnetic field, and there is a hysteresis loop between the warm and the cool branches. According to the equation of $\varepsilon' = Cd/\varepsilon_0 A$, C is the capacity, d is the dimension of the sample between the electrodes, ε_0 is the permittivity of vacuum, and A is the area of the electrode. Here the only variable left in the formula is d, so the drop of the permittivity means the change of the sample dimension. Therefore one can use the above equation to evaluate the extent of the change in d; after a simple mathematical derivation, we get the relationship between the change of d and capacity C in the forms of

$$\frac{\Delta d}{d_{T_0}} = \frac{d(T) - d(T_0)}{d(T_0)} = -\frac{C(T) - C(T_0)}{C(T)}, \quad (1)$$

and

$$\frac{\Delta d}{d_{H_0}} = \frac{d(H) - d(H_0)}{d(H_0)} = -\frac{C(H) - C(H_0)}{C(H)}. \quad (2)$$

Here we assume that A and ε' are constant. According to Eq. (1), the experimental results show that the thickness of the sample (d) is compressed when it goes through T_N, which is related to the structural transition from cubic symmetry to tetragonal symmetry as reported before [1]. In an applied magnetic field of 1 T, ε' is suppressed when $H \perp E$. Conversely, ε' shows a sudden rise when $H \parallel E$, which is almost symmetric to the $H \perp E$ as shown in Fig. 3(a). These results
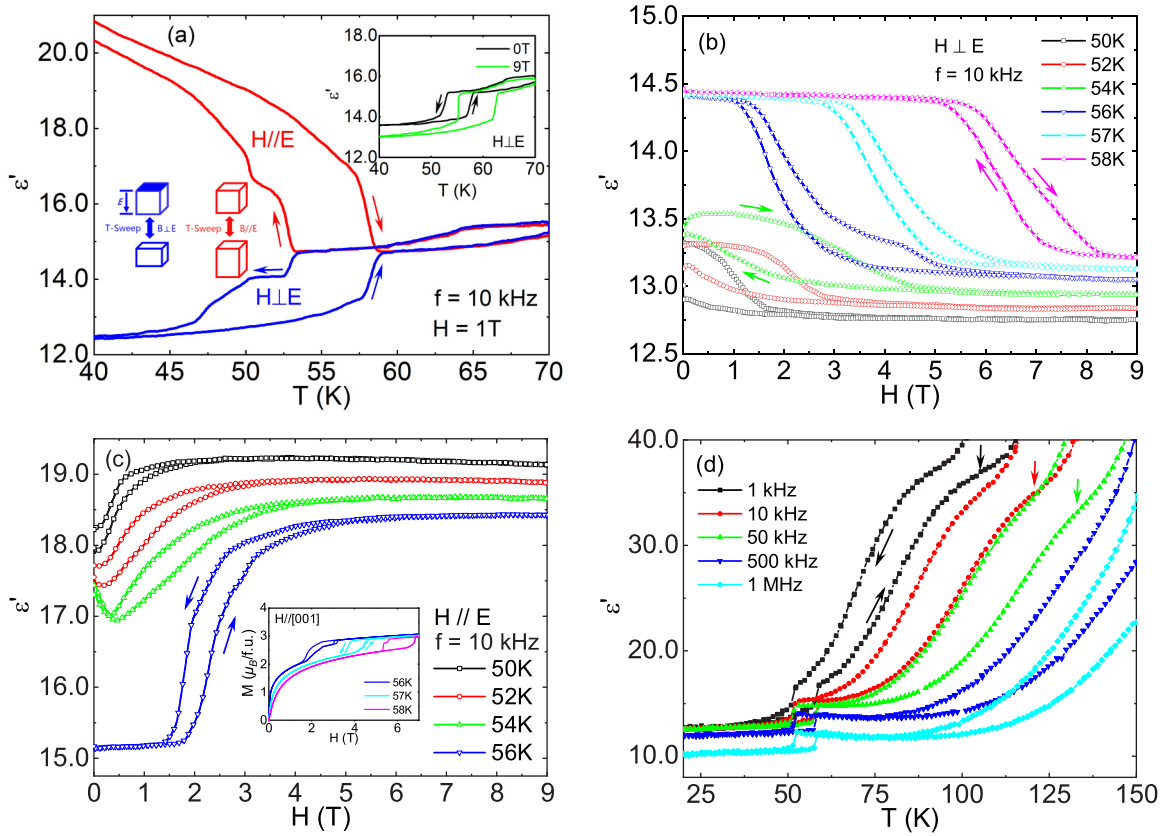
FIG. 3. The temperature dependence of dielectric permittivity of MnV$_2$O$_4$ under $H = 1$ T with a 10 kHz AC electric field for $H \perp E$ and $H \| E$; the inset displays the temperature dependence of dielectric permittivity under zero field and $H = 9$ T. (b), (c) The magnetic-field dependence of isothermal dielectric permittivity for $H \perp E$ and $H \| E$, respectively. The inset in (c) gives the isothermal magnetization for comparison. (d) The temperature dependence of dielectric permittivity of MnV$_2$O$_4$ under different frequencies. The colored arrows represent the position of the plateaulike change.

indicate that the sample thickness can be regularized by an applied magnetic field, which directly confirms the existence of the magnetostriction effect. For a given temperature as shown in Figs. 3(b) and 3(c), significant magnetodielectric behaviors were observed, particularly for the case of the temperature above $T^* \approx 52$ K. For $H \perp E$ ($H \| E$), the external magnetic field gradually decreases (increases) the ε', which then reaches the minimum (maximum) value in the high magnetic-field regime. According to Eq. (2), the results also suggest that MnV$_2$O$_4$ has a strong magnetostriction effect. Then we evaluated the change in d using Eq. (1), Eq. (2), and our experimental data, which yield the minimal $\Delta d/d$ about 11% for temperature dependence measurements and about 3% for magnetic-field dependence measurements. These values are different from our magnetostriction measurements ($\sim$0.3%; see Fig. 4) and the theoretical value (0.63%) [28]. The difference may result from the change of permittivity that reflects not only the change of d but also the change of area A, the contribution of dipole polarization due to the redistribution of the crystal domains of MnV$_2$O$_4$, etc. Furthermore, the critical field of the phase transition shown in Fig. 2(a) [and the inset in Fig. 3(c)] corresponds well to those shown in Figs. 3(b) and 3(c), indicating the existence of the correlation effect between the spin and lattice degrees of freedom in MnV$_2$O$_4$.

In the dielectric measurements, the interfacial effect may introduce nonintrinsic influence into the results. Generally, the dielectric relaxation observed only at relatively low frequencies and high temperatures may be attributed to interfacial Maxwell-Wagner (MW) polarization, space-charge polarization at the interface between the samples and the electrodes, and so on [39]. At high frequency and low temperature, the contribution from interface becomes feeble. Therefore to exclude such effect, permittivity measurements under different frequencies were performed as displayed in Fig. 3(d). At low frequency, the plateaulike changes appear at higher temperatures, which are indicated by the arrows; this plateaulike change moves toward the high-temperature region as the frequency increases and vanishes beyond 50 kHz, and it may arise from the interfacial MW polarization. Here we focus on the temperature around T_N, where the MW polarization is almost suppressed at 10 kHz.

To directly observe the magnetostriction effect of MnV$_2$O$_4$, a series of strain measurements were performed using strain gauges, and the results are shown in Fig. 4. For the case under the static magnetic field, the structure transition occurs at T_N, resulting in changes in lattice parameters, and a small kink occurs near T^*; the results are given in Fig. 4(a). In MnV$_2$O$_4$, compared with the cubic phase, the c_T axis of the tetragonal phase contracts and the ab_T plane expands.
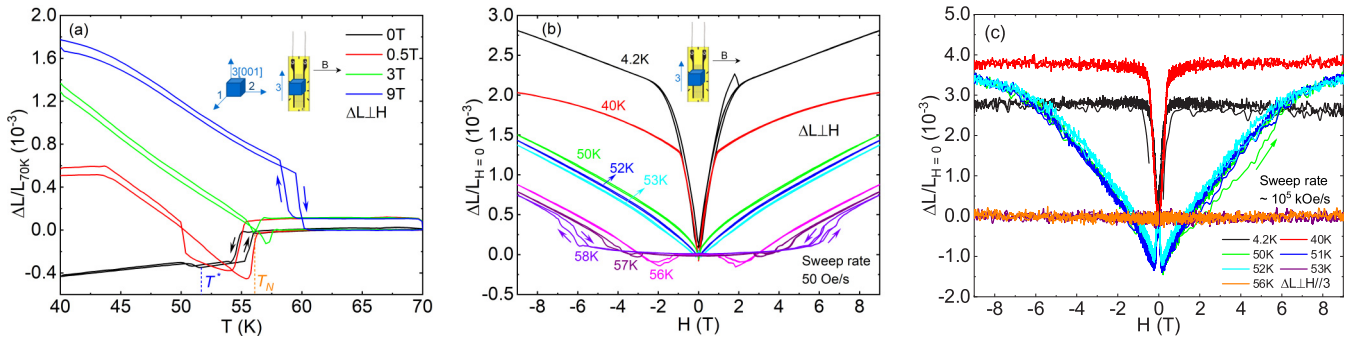
FIG. 4. (a) The temperature dependence of $\Delta L/L$ under different magnetic fields. (b), (c) The magnetic-field dependence of $\Delta L/L$ measured by the static magnetic field and pulsed field, respectively.

Meanwhile, the tetragonal phase can align along any one of the three crystalline axes of the crystal, so there are three types of domains in the tetragonal phase; these domains randomly distribute in the crystal. Under a magnetic field of 0.5 T, the sign of the slope of temperature dependence of $\Delta L/L$ is reversed compared with that without applied magnetic field, indicating that the distribution of the domain can be adjusted by the applied magnetic field [1,28,31]. But the temperature dependence is recovered below ~ 43 K; this implies that the orientation of the domain in tetragonal phase is anisotropic, and the anisotropic energy, magnetic-field energy, and thermal fluctuation compete with each other. When the magnetic field is 3 T, the sign of the slope of temperature dependence of $\Delta L/L$ is completely reversed below T_N. This means, eventually, that the c axis of the tetragonal phase is almost aligned parallel to the magnetic-field direction. Meanwhile, the structural phase-transition temperature gradually increases as the magnetic field increases, which is consistent with that observed in the $\varepsilon' - T$ curves in the inset of Fig. 3(a). As shown in Fig. 4(b), below T^*, $\Delta L/L$ increases almost uniformly with the increase of magnetic field, indicating that a magnetostriction effect exists in MnV_2O_4, and the tetragonal domains are gradually aligned to the magnetic-field direction as the magnetic field increases. Above T^*, an obvious transition with a small strain hysteresis loop occurs, and the critical field increases with the increase of temperature. The same transition process was also observed in Fig. 2(a) and Figs. 3(b) and 3(c). It is noteworthy that at the same temperature, the magnetization and strain share the same critical magnetic field, indicating that the spin-lattice coupling exists in MnV_2O_4.

Figure 4(c) shows the strain measured in the pulsed magnetic field; below T^*, the magnetostrictive change is consistent with that displayed in Fig. 4(b); the difference in the slope of $(\Delta L/L)/H$ between that measured in the pulsed magnetic field and in the static magnetic field is related to the different sweep rate of the magnetic field. Above T^*, no significant magnetostriction behavior was observed, which may be related to the abnormal magnetization in the pulsed magnetic field. In other words, the correlation between magnetization and magnetostriction is closely related to the coupling between spin and lattice degrees of freedom. In addition, the experimental data show that the anomalous magnetostriction behavior appears just above T^*, below which the spin configuration in the V sublattice becomes NCL, indi-

cating that this spin configuration transformation may be the source of the observed anomaly.

In MnV_2O_4, it is well known that the OO that occurred at T_N induces the cubic-to-tetragonal structural transition [1]. The small kink at T^* shown in Fig. 4(a) illustrates that the lattice structure has changed, indicating the change of the orbital state. Previous study has shown that the thermal conductivity of MnV_2O_4 is further recovered below T^*, which also manifests the change of the orbital state [27]. Thus the change of the orbital state plays an important role in the observed magnetostriction anomaly. According to the Kugel-Khomskii model, in orbital active systems, the spin configuration can reflect the orbital state and vice versa [3,4]. It is possible that the orbital states of CL spin configuration and NCL spin configuration are different, so there are two orbital states between T_N and T^*, and the orbital state is unitary below T^*. Based on the experimental results and the above analysis, a possible explanation for the observed abnormal magnetization and magnetostriction behaviors is given below. Above T^*, due to the coexistence of different orbital states, the coupling between spin and orbital degrees of freedom is weak, and the weak interaction makes the magnetic phase transition unable to drive the tetragonal domains synchronously to the field direction in the fast sweep rate of the pulsed magnetic field; that is, only the spin can respond instantly to the change of the external magnetic field. Therefore the change of the magnetostriction was not observed under the pulsed magnetic field. In contrast, the static magnetic field possesses a much slower sweep rate, in which the tetragonal domains have enough time to be aligned to the field direction, so the change of the magnetostriction was observed. Then we suggest that, under the pulsed magnetic field, a quasiadiabatic process was established due to both the rather weak spin-orbital correlation and the fast field sweep rate of the pulsed magnetic field. Below T^*, the spin-orbital correlation effect is enhanced due to the change of orbital state such that the change of the magnetization and magnetostriction behaviors under the pulsed magnetic field is consistent with that under the static magnetic field.

Based on the experimental results shown in Fig. 2(a), the applied magnetic field can induce the NCL spin structure. Therefore it is reasonable to assume that the magnetostriction effect above T_N shown in Fig. 4(b) is also caused by altering the orbital state, namely, the orbitals are partially ordered. Although the NCL structure was realized, the enhanced
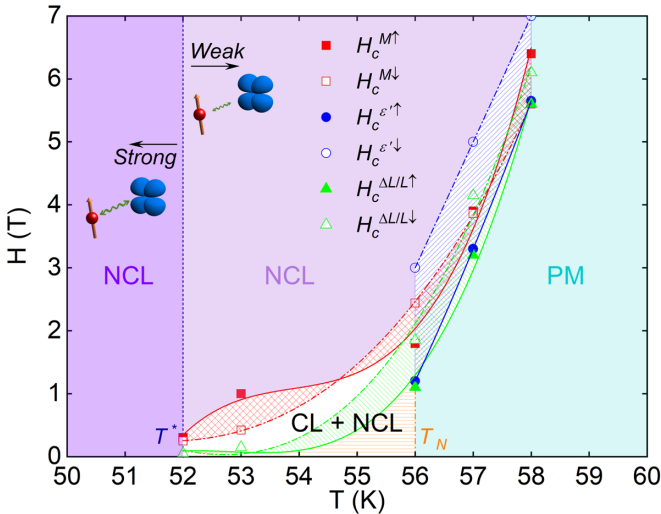
FIG. 5. The phase diagram of the spin configuration of MnV_2O_4 by extracting the critical field (H_c) from the magnetization (M), dielectric permittivity (ε'), and magnetostriction ($\Delta L/L$) measurements. The up (down) arrow represents the field-ascending (-descending) branch of the corresponding measurement, and the color lines represent the phase boundaries. Below T^*, the spin configuration is NCL, which is filled with purple color. The field-induced NCL phase is shown with lavender color. The CL and NCL spin configurations coexist in the striped shaded area. In the PM phase, which is filled with blue-green color, the spin is unpolarized. The inserted cartoons are for illustrating the different spin-orbital interaction strength; below T^*, the spin-orbital correlation effect is strong; above T^*, this correlation effect is weak.

spin-orbital interaction is still insufficient to realize the magnetostriction behavior under the pulsed magnetic field because of the significant thermal fluctuation. For the static magnetic field, the slow sweep rate provides a stable circumstance to realize the magnetostriction behavior, but its $\Delta L/L$ is small. In the meantime, the observed magnetodielectric effect shown in Figs. 3(b) and 3(c) should also be related to the change of orbital state. In MnV_2O_4, the orbital order induces the structural phase transition from cubic to tetragonal. Due to the random distribution of the tetragonal domain, at the boundary of which local Mn-O and V-O bond distortions and charge displacements can give rise to local dipoles which may lead to the change of permittivity [40]. Thus the change of orbital state should result in the change of local dipoles as well, leading to the change of permittivity. However, it is difficult

to evaluate its quantitative contribution due to the coexistence of multiple polarization mechanisms.

The phase diagram was drawn based on measurements of magnetization, magnetostriction, and dielectric permittivity. As shown in Fig. 5, the phase diagram can be divided into three different regions, namely, the PM, the NCL, and the coexistence state of the CL/NCL. Above T^*, the field-induced CL to NCL shows that the NCL is more stable, which can be understood in terms of the frustrated feature of the V^{3+} sublattice. According to the Kugel-Khomskii model, the phase boundaries distinguish not only different spin configurations but also different orbital states. There may be a series of orbital states through the whole temperature region in MnV_2O_4, including the high-temperature orbital disordered state, orbital glass state activated by the JT effect between T_N and T^*, and the further ordered glasslike orbital state or completely orbital ordered state below T^*, and these states are highly related to the frustrated feature of the pyrochlore lattice. These orbital states in turn correspond to the PM, CL/NCL coexisting, and NCL regions that are shown in Fig. 5. Yet the true nature of the orbital states in MnV_2O_4 and their coupling with the spin needs further investigation.

IV. CONCLUSION

In summary, MnV_2O_4 exhibits exotic properties including the anisotropic magnetic susceptibility, anisotropic dielectric permittivity, and the magnetostriction effect. The NCL spin configuration can be realized by applying a magnetic field above T_N. Especially, the magnetization and magnetostriction phenomena observed in the pulsed magnetic field are totally different from those observed in the static magnetic field. Based on the assumption of the weak interaction between spin and V-t_{2g} orbitals, above T^*, the magnetization process in the pulsed magnetic field is quasiadiabatic; that is, the evolution of the spin under the magnetic field is instantaneous. However, the crystal domain cannot respond to the high sweep rate of the pulsed magnetic field. Below T^*, the spin-orbital interaction is stronger due to the change of the orbital state; the crystal domain can also respond to the pulsed magnetic field instantaneously. The results show that this compound provides an ideal playground to study the dynamic response of the weak spin-orbital interaction in the t_{2g} orbitals.

[1] T. Suzuki, M. Katsumura, K. Taniguchi, T. Arima, and T. Katsufuji, Phys. Rev. Lett. **98**, 127203 (2007).

[2] J. B. Goodenough, Phys. Rev. **100**, 564 (1955).

[3] K. Kugel and D. Khomskii, Zh. Eksp. Teor. Fiz. **64**, 1429 (1973).

[4] K. I. Kugel and D. I. Khomskii, Sov. Phys. Usp. **25**, 231 (1982).

[5] S. Bhattacharjee, S. Zherlitsyn, O. Chiatti, A. Sytcheva, J. Wosnitza, R. Moessner, M. E. Zhitomirsky, P. Lemmens, V. Tsurkan, and A. Loidl, Phys. Rev. B **83**, 184421 (2011).

[6] Y. Nii, H. Sagayama, T. Arima, S. Aoyagi, R. Sakai, S. Maki, E. Nishibori, H. Sawa, K. Sugimoto, H. Ohsumi, and M. Takata, Phys. Rev. B **86**, 125142 (2012).

[7] Y. Nii, H. Sagayama, H. Umetsu, N. Abe, K. Taniguchi, and T. Arima, Phys. Rev. B **87**, 195115 (2013).

[8] S. Blanco-Canosa, F. Rivadulla, V. Pardo, D. Baldomir, J.-S. Zhou, M. García-Hernández, M. A. López-Quintela, J. Rivas, and J. B. Goodenough, Phys. Rev. Lett. **99**, 187201 (2007).

[9] D. Choudhury, T. Suzuki, D. Okuyama, D. Morikawa, K. Kato, M. Takata, K. Kobayashi, R. Kumai, H. Nakao, Y. Murakami, M. Bremholm, B. B. Iversen, T. Arima, Y. Tokura, and Y. Taguchi, Phys. Rev. B **89**, 104427 (2014).

[10] G. Giovannetti, A. Stroppa, S. Picozzi, D. Baldomir, V. Pardo, S. Blanco-Canosa, F. Rivadulla, S. Jodlauk, D. Niermann, J. Rohrkamp, T. Lorenz, S. Streltsov, D. I. Khomskii, and J. Hemberger, Phys. Rev. B **83**, 060402(R) (2011).

[11] A. Kismarahardja, J. S. Brooks, H. D. Zhou, E. S. Choi, K. Matsubayashi, and Y. Uwatoko, Phys. Rev. B **87**, 054432 (2013).

[12] A. Kiswandhi, J. S. Brooks, J. Lu, J. Whalen, T. Siegrist, and H. D. Zhou, Phys. Rev. B **84**, 205138 (2011).

[13] J. Krishna, N. Singh, S. Shallcross, J. K. Dewhurst, E. K. U. Gross, T. Maitra, and S. Sharma, Phys. Rev. B **100**, 081102(R) (2019).

[14] J. Ma, J. H. Lee, S. E. Hahn, T. Hong, H. B. Cao, A. A. Aczel, Z. L. Dun, M. B. Stone, W. Tian, Y. Qiu, J. R. D. Copley, H. D. Zhou, R. S. Fishman, and M. Matsuda, Phys. Rev. B **91**, 020407(R) (2015).

[15] T. Omura, T. Ishikawa, Y. Ishitsuka, and T. Katsufuji, Phys. Rev. B **86**, 054436 (2012).

[16] V. Pardo, S. Blanco-Canosa, F. Rivadulla, D. I. Khomskii, D. Baldomir, H. Wu, and J. Rivas, Phys. Rev. Lett. **101**, 256403 (2008).

[17] S. Sarkar, T. Maitra, R. Valentí, and T. Saha-Dasgupta, Phys. Rev. Lett. **102**, 216405 (2009).

[18] W. Wu, Phys. Rev. B **91**, 195108 (2015).

[19] Q. Zhang, K. Singh, F. Guillou, C. Simon, Y. Breard, V. Caignaert, and V. Hardy, Phys. Rev. B **85**, 054405 (2012).

[20] Z. Zhang, D. Louca, A. Visinoiu, S.-H. Lee, J. D. Thompson, T. Proffen, A. Llobet, Y. Qiu, S. Park, and Y. Ueda, Phys. Rev. B **74**, 014108 (2006).

[21] H. Katsura, N. Nagaosa, and A. V. Balatsky, Phys. Rev. Lett. **95**, 057205 (2005).

[22] L. M. Rodríguez-Martínez and J. P. Attfield, Phys. Rev. B **63**, 024424 (2000).

[23] M. v. Zimmermann, J. P. Hill, D. Gibbs, M. Blume, D. Casa, B. Keimer, Y. Murakami, Y. Tomioka, and Y. Tokura, Phys. Rev. Lett. **83**, 4872 (1999).

[24] S. V. Streltsov and D. I. Khomskii, Phys.-Usp. **60**, 1121 (2017).

[25] Y. Tokura and N. Nagaosa, Science **288**, 462 (2000).

[26] V. O. Garlea, R. Jin, D. Mandrus, B. Roessli, Q. Huang, M. Miller, A. J. Schultz, and S. E. Nagler, Phys. Rev. Lett. **100**, 066404 (2008).

[27] Q.-Y. Liu, Z.-Y. Liu, X.-B. Zhou, T. Yajima, Y. Uwatoko, J.-G. Cheng, L. Tao, Z.-G. Liu, M.-X. Huo, X.-J. Wang, and Y. Sui, Phys. Rev. B **100**, 224418 (2019).

[28] Q.-Y. Liu, Y. Ma, Y. Sun, Z.-Y. Liu, J.-G. Cheng, X.-B. Zhou, L. Tao, M.-X. Huo, X.-J. Wang, and Y. Sui, Phys. Rev. B **102**, 144404 (2020).

[29] K. Matsuura, H. Sagayama, A. Uehara, Y. Nii, R. Kajimoto, K. Kamazawa, K. Ikeuchi, S. Ji, N. Abe, and T.-h. Arima, Phys. Rev. Lett. **119**, 017201 (2017).

[30] Y. Murakami, Y. Nii, T. Arima, D. Shindo, K. Yanagisawa, and A. Tonomura, Phys. Rev. B **84**, 054421 (2011).

[31] Y. Nii, N. Abe, K. Taniguchi, and T. Arima, Appl. Phys. Lett. **100**, 051905 (2012).

[32] R. Singh, T. Hansen, C. Ritter, N. Sharma, P. Shahi, S. Chatterjee, and A. Das, J. Phys.: Condens. Matter **29**, 345802 (2017).

[33] K. Adachi, T. Suzuki, K. Kato, K. Osaka, M. Takata, and T. Katsufuji, Phys. Rev. Lett. **95**, 197202 (2005).

[34] K. Myung-Whun, J. S. Kim, T. Katsufuji, and R. K. Kremer, Phys. Rev. B **83**, 024403 (2011).

[35] H. Ueda, H. A. Katori, H. Mitamura, T. Goto, and H. Takagi, Phys. Rev. Lett. **94**, 047202 (2005).

[36] See Supplemental Material at http://link.aps.org/supplemental/10.1103/PhysRevB.105.054401 for field sweep rate measurements in pulsed magnetic field, angular dependence of dielectric permittivity measurements and magnetostriction measurements for different field directions and crystalline axes.

[37] E. P. Wohlfarth, J. Phys. F: Met. Phys. **14**, L155 (1984).

[38] P. Bruno, G. Bayreuther, P. Beauvillain, C. Chappert, G. Lugert, D. Renard, J. P. Renard, and J. Seiden, J. Appl. Phys. **68**, 5759 (1990).

[39] P. Lunkenheimer, S. Krohns, S. Riegg, S. G. Ebbinghaus, A. Reller, and A. Loidl, Eur. Phys. J.: Spec. Top. **180**, 61 (2009).

[40] P. Mondal, D. Bhattacharya, and P. Choudhury, J. Phys.: Condens. Matter **18**, 6869 (2006).